

Query Training: Learning and inference for directed and undirected graphical models

Miguel Lázaro-Gredilla*, Wolfgang Lehrach*, Nishad Gothoskar*, Guangyao Zhou*,
Antoine Dedieu*, Dileep George*
Vicarious AI

Abstract

Probabilistic graphical models (PGMs) provide a compact representation of knowledge that can be queried in a flexible way: after learning the parameters of a graphical model, new probabilistic queries can be answered at test time without re-training. However, learning undirected graphical models is notoriously hard due to the intractability of the partition function. For directed models, a popular approach is to use variational autoencoders, but there is no systematic way to choose the encoder architecture given the PGM, and the encoder only amortizes inference for a single probabilistic query (i.e., new queries require separate training). We introduce Query Training (QT), a systematic method to turn any PGM structure (directed or not, with or without hidden variables) into a trainable inference network. This single network can approximate any inference query. We demonstrate experimentally that QT can be used to learn a challenging 8-connected grid Markov random field with hidden variables and that it consistently outperforms the state-of-the-art AdvIL when tested on three undirected models across multiple datasets.

1 Introduction

In machine learning we are interested in discovering regularities in data that allow us to perform inference about novel data points. A paradigmatic example are neural networks (NNs). In most practical cases, a NN is a parametric function, structured in layers, that deterministically produces an output given the input. By minimizing an appropriate loss function on input-output pairs, we expect it to learn a mapping that generalizes to new cases. Recent years have seen a big success in the training of fairly complex and deep NNs using stochastic gradient descent (SGD). Tools like PyTorch [Paszke et al., 2019] and TensorFlow [Abadi et al., 2015] make this process straightforward.

When a probabilistic graphical model (PGM) is used to model a dataset, there is no notion of input or output. Instead, these can be arbitrarily chosen at test time by conditioning on available data. Such a PGM captures more information about the data than a NN, for which the inputs and outputs are prefixed. Ideally, the PGM captures the full statistical description, up to model mismatches. After learning a PGM, we can query it to provide an estimation of any subset of variables given the rest (with varying degrees of uncertainty). NNs are limited to answering a single query, the one that they were trained for. Flexible querying is a requirement in all but the simplest artificial intelligence agents, which need to deal with uncertainty and cannot afford separate NNs for each possible query. Thus, PGMs are more suited as a compact knowledge representation that admits flexible querying.

Despite this advantage, PGMs are not without difficulties in practice. Namely, learning (optimizing the parameters of the PGM to best match observed data) and inference (the aforementioned flexible querying) are intractable for most models of interest, even fairly simple ones. Learning the parameters of an undirected PGM with hidden variables using maximum likelihood (ML) is a notoriously difficult

*Email: {miguel,wolfgang,nishad,stannis,antoine,dileep}@vicarious.com

problem [Welling and Sutton, 2005, Kuleshov and Ermon, 2017, Li et al., 2019]. When all variables are observed, the range of applicable techniques is broadened [Sutton and McCallum, 2005, Sutton and Minka, 2006, Sutton and McCallum, 2007, Bradley, 2013], but the problem remains intractable in general. When hidden variables are present, the intractability is twofold: (a) integrating out the hidden variables (also a challenge in directed models) and (b) computing the partition function. The second problem is generally considered harder [Welling and Sutton, 2005]. Unfortunately, for images and other data types, undirected PGMs offer the most compact representation, so using only directed PGMs is not a general enough solution. We will thus focus on *undirected* PGMs in this work.

Often PGMs and NNs work together. NNs (shallow or deep) can be used either as a link function in the definition of PGMs or as an amortized inference network² to accelerate learning. This is the case in variational autoencoders (VAEs, Kingma and Welling [2013]), pixel convolutional neural networks (PixelCNNs, Van Oord et al. [2016]), etc. But these architectures inherit the shortcomings of NNs: despite the presence of an underlying PGM, flexible querying without retraining is not supported. VAE’s encoder can only compute the posterior over the hidden units and fails to do so if some of the inputs are missing. Similarly, PixelCNNs are trained on a specific (forward) order, and can answer forward inpainting queries, but cannot handle backward queries, or queries with uncertain inputs.

Contribution The aim of this work is to provide a systematic framework to turn any PGM into an inference network that enjoys benefits from both PGMs and NNs. Our approach (a) supports flexible *marginal* querying without retraining; (b) provides a simple mechanism for training and inference, with no need to estimate the partition function; and (c) handles both directed and undirected PGMs. We will focus our experiments on the harder case of undirected PGMs.

2 Query training (QT)

Our approach takes an (untrained) PGM and unrolls it into a single NN to answer arbitrary queries. It then trains the weights of the NN using different types of queries. The resulting NN can be used at test time for flexible querying, as if it was a PGM. We call this approach query training (QT).

2.1 Queries that need to be answered

Given a knowledge representation of some type (e.g. PGM) for the set of variables $\mathbf{x} = \{x_1, \dots, x_N\}$, we want to be able to compute conditional marginal probabilistic queries of the form

$$p(x_{\text{output}} | \{x_i\}_{i:\text{input}}), \forall \text{output} \in \{1, \dots, N\}, \forall \text{input} \subset \{1, \dots, N\} \quad (1)$$

where x_{output} is a single variable, and “input” is a *subset* of the remaining variables. Any variables that do not correspond to the input nor the output are marginalized out in the above query.

Queries which do not fit Eq. (1) directly (e.g., the joint distribution of two output variables) can be decomposed as a combination of conditional marginal queries by using the chain rule of probability. So a system that is able to answer queries like Eq. (1) provides enough information to resolve any probabilistic query, with the number of queries being linear in the number of output variables³.

A brute force solution would be to consider each of these queries its own regression problem and train separate NNs. However, the number of different queries of this type is exponential in the number of variables, so this would be infeasible. Also, we know that those regressions are not independent, so we would be losing statistical power. Ideally, we would like to train a single NN that can be reconfigured to address different queries. To this end, we will follow approximate inference in PGMs.

2.2 Approximate inference in PGMs

Probabilistic queries in PGMs are in most cases intractable, so approximations such as loopy belief propagation (BP, Murphy et al. [2013]) or variational inference (VI, Blei et al. [2017]) are used. These approximations are invariant to scale, so the computation of the partition function is *not needed*.

²Note that the inference network is typically designed independently of the generative model, despite both being tightly coupled.

³If the answers to these queries is approximate (as it will be the case with QT), different factorizations of a joint density will result in different approximations.

Loopy BP and VI can be cast as optimization problems. As such, they rarely have a closed-form solution and are instead solved iteratively, which is computationally intensive. To address this problem, amortized inference can be used. A prime example of this are VAEs [Kingma and Welling, 2013]: a learned function (typically an NN) is combined with the reparameterization trick [Rezende et al., 2014, Titsias and Lázaro-Gredilla, 2014] to compute the posterior over the hidden variables given the visible ones. Although a VAE performs inference faster than VI optimization, a single predefined query can be solved. In contrast, BP and VI answer arbitrary queries (albeit with more compute). Also note that standard VAEs can only handle directed PGMs, and a more sophisticated variational apparatus with multiple NNs [Li et al., 2019] is required for undirected PGMs.

BP and VI are closely connected, but behave differently. For instance, for tree PGMs, parallel BP converges to the exact solution in a number of steps equal to the diameter of the tree [Murphy et al., 2013], whereas VI will in general take much longer to converge. In general, parallel BP tends to produce higher quality marginals in less iterations, so we will choose it over VI in this work.

2.3 An intuitive description of query training

BP gives a recipe to compute any marginal query of the form of Eq. (1), while sharing the same parameters for all queries. We can then consider the loopy BP, unrolled over a fixed set of iterations, as our inference NN. This NN takes an additional input specifying the desired query. Instead of starting with a trained PGM and generating the inference NN (which is certainly possible), we could generate a “blank” inference NN from an untrained PGM and then learn its (single set of) parameters by minimizing the cross-entropy (CE) of its predictions over both data points and queries. This would hopefully generalize to new data points and new queries never seen at training time. The intuition behind the existence of a single NN parameterization that approximately satisfies all the queries comes from the good results of running BP on a correct PGM, which uses a single set of parameters. Note that the the same set of parameters (weights) are shared across all inference steps (layers).

Minimizing the CE between the training data and the query predictions with respect to the model parameters is *not* equivalent to maximum likelihood learning. However, we have derived consistency results (see Supplementary Material) for general exponential family models, analogous to those of pseudolikelihood [Hyvärinen, 2006], showing that our CE loss is reasonable.

The computation of the partition function is sidestepped, so undirected PGMs can be used just as easily: normalization is only required for the output variable of each query, i.e., in one dimension.

Loopy BP is in general only approximate, so one cannot expect predictions to be exact or even necessarily consistent (e.g., the query product $p(x = 0|y = 1)p(y = 1)$ is not guaranteed to be identical to the query product $p(y = 1|x = 0)p(x = 0)$, although the cost function will tend to make both similar). On the plus side, the training is free to select the parameters that produce the most precise inference over the training queries, as opposed to the parameters that are closest to the original PGM, so the training procedure can compensate for shortcomings in the BP approximation.

2.4 Training the inference network

The starting point is an unnormalized PGM parameterized by θ . Its probability density can be expressed as $p(\mathbf{x}; \theta) = p(\mathbf{v}, \mathbf{h}; \theta) \propto \exp(\phi(\mathbf{v}, \mathbf{h}; \theta))$, where \mathbf{v} are the visible variables available in our data and \mathbf{h} are the hidden variables. A query is a binary vector \mathbf{q} of the same dimension as \mathbf{v} that partitions the visible variables in two subsets: one for which (possibly soft) evidence is available (inputs) and another whose marginal probability we want to estimate (outputs). Note that we want to compute the marginal of each selected output given all the inputs, independently, that is, for $\mathcal{S} = \{i : q_i = 1\}$, we want to compute all the marginal queries $p(x_i | \{x_j\}_{j \in \mathcal{S}})$, $\forall i \notin \mathcal{S}$.

The query-trained neural network (QT-NN) follows from specifying a graphical model $\phi(\mathbf{v}, \mathbf{h}; \theta)$, a temperature T and a number of inference timesteps N over which to run parallel BP. The general equations of the QT-NN are given next in Section 2.5.

In Fig. 1, a QT-NN takes as input a sample \mathbf{v} from the dataset and a random query mask \mathbf{q} . The query \mathbf{q} blocks the network from accessing the “output” variables, and instead only offers access to the “input” variables. The variables assigned to inputs and outputs change with each query \mathbf{q} drawn. The QT-NN produces as output an estimate of the marginal probabilities $\hat{\mathbf{v}}$ for the whole input sample. Obviously, we only care about how well the network estimates the variables that it did

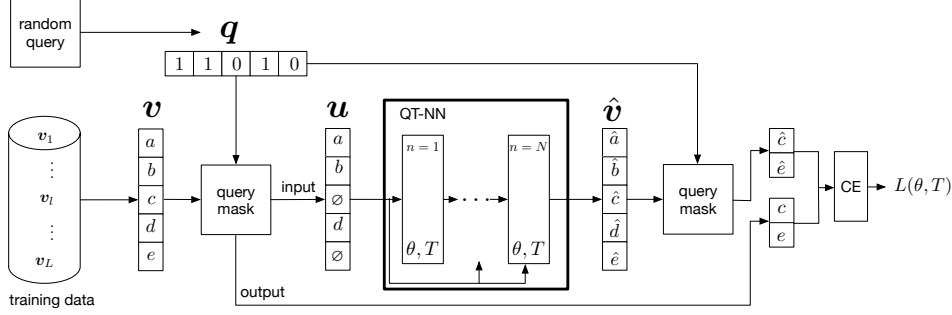


Figure 1: One step of query training. A random sample from the training data is split according to a random query mask in input and output dimensions. The input is processed inside the QT by N identical stages, producing an estimation of the marginal probabilities from the sample. The loss function considers the cross-entropy between the true and estimated marginals. Training uses stochastic samples from both training data and training queries.

not see at the input. So we measure how well \hat{v} matches the correct v in terms of cross-entropy (CE), but only for the variables that q regards as “output”.

Taking expectation wrt v and q , we get $L(\theta, T) = \mathbb{E}_{v, q}[\text{CE}_q(v, \hat{v})]$, the loss function that we use to train the QT-NN, where the estimated visible units are given by $\hat{v} = \text{QT-NN}(v, q; \theta, T)$.

We minimize this loss wrt θ, T via SGD, sampling from the training data and some query distribution. The query distribution can be uniform, or a function of the problem structure. The number of QT-NN layers N is fixed a priori. We term this approach query training (QT).

One can think of the QT-NN as a more flexible version of the encoder in a VAE: instead of hardcoding inference for a single query (normally, hidden variables given visible variables), the QT-NN also takes as input a mask q specifying which variables are observed, and provides inference results for unobserved ones. Note that h is never observed, and instead approximately marginalized over by BP.

2.5 Unrolling BP into a QT-NN

For a given set of graphical model parameters θ and temperature T we derive a feed-forward function that approximately resolves arbitrary inference queries by unrolling the parallel BP equations for N iterations. First, we combine the available evidence v and the query q into a set of unary factors. Unary factors specify a probability density function over a variable. Therefore, for each dimension inside v that q labels as “input”, we provide a (Dirac or Kronecker) delta centered at the value of that dimension. For the “output” dimensions and hidden variables h we set the unary factor to an uninformative, uniform density. Finally, soft evidence, if present, can be incorporated through the appropriate density function. The result of this process is a unary vector of factors u that only contains informative densities about the inputs and whose dimensionality is the sum of the dimensionalities of v and h . Each dimension of u will be a real number for binary variables (which we encode in the logit space), and a full distribution in the general case.

Once v and the query q are encoded in u , we can write down the equations of parallel BP over iterations as an NN with N layers, i.e., the QT-NN. To simplify notation, let us consider a PGM that contains only pairwise factors. By mapping the messages to the log-space, the predictions of the QT-NN and the messages from each layer to the next can be written as

$$\begin{aligned} \hat{v}_i &= \text{softmax}\left(\theta_i + u_i + \sum_k m_{ki}^{(N)}\right) & m_{ij}^{(n)} &= f_{\theta_{ij}}\left(\theta_i + u_i + \sum_{k \neq j} m_{ki}^{(n-1)}; T\right) & m_{ij}^{(0)} &= 0 \\ \hat{v} &= g_{\theta}(\mathbf{m}^{(N)}, \mathbf{u}) & \mathbf{m}^{(n)} &= f_{\theta}(\mathbf{m}^{(n-1)}, \mathbf{u}; T) & \mathbf{m}^{(0)} &= 0, \end{aligned}$$

where the second row express the same equations as the first row, but in vectorized format.

Here $\mathbf{m}^{(n)}$ collects all the messages⁴ that exit layer $n - 1$ and enter layer n . Messages have direction, so $m_{ij}^{(n)}$ is different from $m_{ji}^{(n)}$ ⁵. Observe how the input term \mathbf{u} is re-fed at every layer. The output of the network is a belief \hat{v}_i for each variable i , which is obtained by a softmax in the last layer. All these equations follow from unrolling BP over iterations, with its messages encoded in log-space.

The portion of the parameters θ relevant to the factor between variables i and j is represented by $\theta_{ij} = \theta_{ji}$, and the portion that only affects variable i is contained in θ_i . Observe that all layers share the same parameters. The functions $f_{\theta_{ij}}(\cdot)$ are directly derived from $\phi(\mathbf{x}; \theta)$ using the BP equations, and therefore inherit its parameters. Finally, parameter T is the “temperature” of the message passing, and can be set to $T = 1$ to retrieve the standard sum-product belief propagation or to 0 to recover max-product belief revision. Values in-between interpolate between sum-product and max-product and increase the flexibility of the NN. See the Supplementary Material for the precise equations obtained when applied to three popular undirected models used in our experiments.

2.6 Connection with pseudo-likelihood

If the distribution over queries only contains queries with a single variable assigned as output (and the rest as input), and there are no hidden variables, the above cost function reduces to pseudo-likelihood training [Besag, 1975]. Query training is superior to pseudo-likelihood (PL) in two ways. Firstly, it provides an explicit mechanism for handling hidden variables. Secondly and more importantly, it preserves learning in the face of high correlations in the input data, which results in catastrophic failure when using PL. If two variables a and b are highly correlated, PL will fail to learn the weaker correlation between a and z , since b will always be available during training to predict a , rendering any correlation with z useless at training time. If at test time we want to predict a from z because b is not available, the prediction will fail. In contrast, query training removes multiple variables from the input, driving the model to better leverage all available sources of information.

Table 1: Comparison of QT-NN, PCD and AdvIL on RBM and DBM. Measurements are NCE, lower is better. QT achieves significantly lower NCE for most datasets compared to the state-of-the-art.

Method	Model	Adult	Conn4	Digits	DNA	Mushr	NIPS	OCR	RCV1	Web
AdvIL-BP	RBM	0.224	0.248	0.530	0.778	0.192	0.795	0.470	0.475	0.142
AdvIL-Gibbs	RBM	0.229	0.238	0.493	0.782	0.218	0.797	0.471	0.477	0.163
PCD-BP	RBM	0.215	0.285	0.530	0.763	0.159	0.801	0.428	0.457	0.140
PCD-Gibbs	RBM	0.218	0.288	0.516	0.765	0.159	0.804	0.427	0.458	0.144
QT (Ours)	RBM	0.167	0.148	0.472	0.766	0.124	0.787	0.377	0.452	0.133
AdvIL-BP	DBM	0.242	0.364	0.578	0.805	0.224	0.816	0.490	0.480	0.146
AdvIL-Gibbs	DBM	0.244	0.299	0.529	0.560	0.690	0.934	0.923	0.568	0.195
QT (Ours)	DBM	0.169	0.146	0.471	0.765	0.124	0.787	0.379	0.453	0.133

3 Experiments

Early works in learning undirected PGMs relied on contrastive energies [Hinton, 2002, Welling and Sutton, 2005]. More recent approaches are NVIL [Kuleshov and Ermon, 2017] and AdvIL [Li et al., 2019], with the latter being regarded as superior. We will use it as our main benchmark.

In this section we first test QT as an approach for learning and querying from undirected PGMs, comparing it with AdvIL on 3 different types of undirected PGMs (using both discrete and continuous variables) and a total of 10 datasets. These models and datasets are exactly the ones used in AdvIL’s paper [Li et al., 2019]. Then we try QT on a challenging grid Markov random field.

3.1 Comparison with AdvIL

All models are trained using uniform random query distribution, i.e., in each SGD step, each variable is independently assigned as input or output with 0.5 probability. We report the test normalized

⁴For a fully connected graph, the number of messages is quadratic in the number of variables, showing the advantage of a sparse connectivity pattern, which can be easily encoded in the PGM architecture.

⁵In the general case, $m_{ij}^{(n)}$ and θ_i are vectors. We only encode matrix in bold, to represent aggregate messages

cross-entropy (NCE) in bits to measure generalization to new data *and new queries*. We normalize the number of predicted variables, so the NCE is the average CE per-variable. The query distribution at test time is the same as the training one, but the actual queries are with high probability unseen in training. Experiments are run on a single Tesla V100 GPU.

The QT-NN equations for the models in this section (which follow from unfolding BP on each PGM) and code to reproduce our results can be found in the Supplementary Material.

3.1.1 Restricted Boltzmann machine (RBM)

We first test QT on which is arguably the simplest undirected model, the RBM. The log-probability of an RBM⁶ is proportional to $\phi(\mathbf{v}, \mathbf{h}; \theta) = 2\mathbf{h}^\top W \mathbf{v} + \mathbf{h}^\top (\mathbf{c}_H - W \mathbf{1}_V) + \mathbf{v}^\top (\mathbf{c}_V - W^\top \mathbf{1}_H)$. We use exactly the same datasets and preprocessing used in the AdvIL paper, with the same hidden layer sizes, check Li et al. [2019] for further details. Since all the variables are binary, a trivial uniform undirected model would result in an NCE of 1 bit.

We also include results from persistent contrastive divergence (PCD), which is known to be very competitive for RBM training [Tieleman, 2008, Marlin et al., 2010]. In fact, AdvIL does not do much better than PCD on this model.

Computing the test NCE for QT is equivalent to running the trained QT-NN on test data, since that is its loss function. PCD and AdvIL, however, do not provide any mechanism to solve arbitrary inference queries, so we needed to resort to slow Gibbs sampling in the learned model, which is much slower. Alternatively, we also tried copying the RBM weights learned by PCD and AdvIL into the QT with $T = 1$ and report those results as PCD-BP and AdvIL-BP.

For AdvIL we use the code provided by the authors. For PCD and QT the validation set is used to choose the learning rate and for early stopping, separately for each dataset. The learning rates considered are $\{0.03, 0.1, 0.3, 1, 3\}$ for PCD and $\{0.001, 0.003, 0.01, 0.03\}$ for QT. For PCD we use `scikit-learn` [Pedregosa et al., 2011]. For QT we unfold BP in $N = 10$ layers and use ADAM [Paszke et al., 2019, Kingma and Ba, 2014] with minibatches of size 500. The T parameter is learned during training. The results are shown in Table 1. Results average 5 independent runs.

QT produces significantly better results for most datasets (marked in boldface), showing that it has learned to generalize to new probabilistic queries on unseen data.

3.1.2 Deep Boltzmann machine (DBM)

For our second experiment, we use a slightly more sophisticated undirected PGM, a DBM with two hidden layers. The log-probability of a DBM⁷ is proportional to $\phi(\mathbf{v}, \mathbf{h}; \theta) = 2\mathbf{h}_2^\top W_{H_2 H_1} \mathbf{h}_1 + 2\mathbf{h}_1^\top W_{H_1 V} \mathbf{v} + \mathbf{h}_2^\top (\mathbf{c}_{H_2} - W_{H_2 H_1} \mathbf{1}_{H_1}) + \mathbf{v}^\top (\mathbf{c}_V - W_{H_1 V}^\top \mathbf{1}_{H_1}) + \mathbf{h}_1^\top (\mathbf{c}_{H_1} - W_{H_2 H_1}^\top \mathbf{1}_{H_2} - W_{H_1 V}^\top \mathbf{1}_V)$. The datasets are the same as for the RBM. The DBM structure (number of units in each hidden layer) for each dataset is identical to that of Li et al. [2019], and we reuse exactly the same process and parameters as in the previous experiment. The results are summarized in Table 1.

QT produces the best performance (marked in boldface) on 8 out of the 9 tested datasets. It is interesting to note that, although inference becomes more challenging for DBM than for RBM (as demonstrated by the generally higher NCEs on most datasets for AdvIL-BP and AdvIL-Gibbs), the performance of QT remains essentially unchanged for DBM as compared with RBM. This suggests that QT not only learns to generalize to new probabilistic queries on unseen data, but also remains highly effective for models where inference becomes more challenging.

3.1.3 Gaussian Restricted Boltzmann machine (GRBM)

Finally, we compare QT with AdvIL on learning a GRBM on the Frey faces dataset. The log-probability of a GRBM is proportional to $\phi(\mathbf{v}, \mathbf{h}; \theta) = -\frac{1}{2\sigma^2} \|\mathbf{v} - \mathbf{b}\|^2 + \mathbf{c}^\top \mathbf{h} + \frac{1}{\sigma} \mathbf{h}^\top W \mathbf{v}$. The hidden units are binary and the visible units are continuous. We follow Li et al. [2019], and fix $\sigma = 1$. The dimensions of \mathbf{h} and \mathbf{v} are respectively 200 and 560 (corresponding to a 28×20 image).

⁶This parameterization is in one-to-one correspondence with the standard and results in simpler QT-NN equations as shown in the Supplementary Material. Most readers can ignore this detail.

⁷See previous footnote.

We train AdvIL using the provided authors’ code. For QT we unfold BP in $N = 50$ layers and use ADAM with learning rate 5×10^{-3} . In the GRBM, BP will send continuous messages to the visible units, and we follow the standard practice of expectation propagation [Minka, 2001] of characterizing those messages as Gaussians. This results in deterministic and differentiable message updates. For further details, see the Supplementary Material.

Since no quantitative results are provided in Li et al. [2019], we create our own by using the preexisting train-test split in the dataset of 1572 and 393 images, respectively. Since there is no validation split, for QT we simply stop training after 50 epochs (training performance has plateaued and we see no signs of overfitting). For AdvIL, we train for 100,000 iterations and save a checkpoint every 100 iterations. We observe overfitting, so we decided to give the competing method an additional advantage and we report the results of the checkpoint that results in the best test set performance. Like in the previous experiments, the results for AdvIL are obtained both by using Gibbs sampling and by transferring its learned weights to a QT in which we run $N = 50$ BP iterations. The NCE for each of the models are Advil-Gibbs: 1.545, Advil-BP: 1.542, and QT: **1.503**. The NCE of a trivial independent Gaussian model using the empirical mean and variance of the training pixels is 1.909. Again, QT produces better results than AdvIL, showing that it can be applied to continuous PGMs.

Testing on significantly different queries. In addition, we assess the ability of QT to answer inference queries whose statistics are significantly different from those seen at training time. In all the models in this section, we train by assigning each variable as input or output with 0.5 probability. We will now, at test time, make queries on images to complete contiguous patches of 5×5 pixels given the rest of the image. The NCE for each of the models are: Advil-Gibbs: 1.525, Advil-BP: 1.530, and QT: **1.493**. The NCE of the trivial model is 1.889. Qualitatively, we find that QT is able to produce image completions that are almost indistinguishable from the original images (shown in Fig 2a).

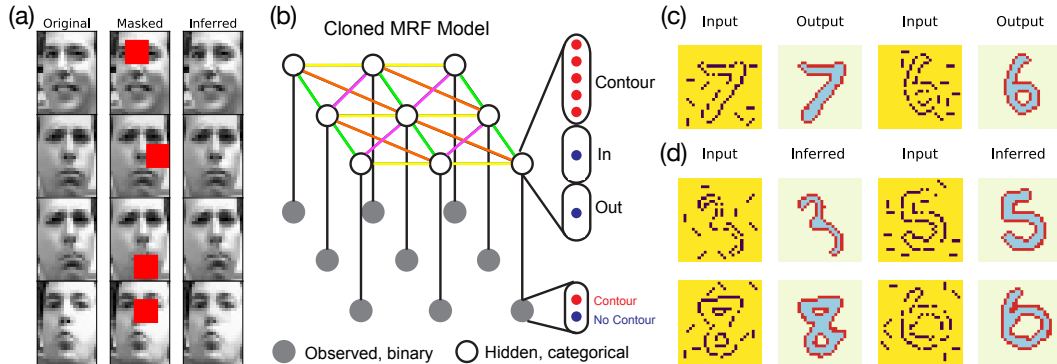


Figure 2: (a) QT can accurately complete masked regions of an image even though it was trained for significantly different queries. (b) An 8-connected cloned Markov random field. Identical factors are shown using the same color. Actual size is 30×30 . (c) Two examples of training pairs: a noisy input digit and its corresponding ground truth segmentation (d) Test data: noisy input digits and their inferred segmentation by the QT-NN (which is obtained unrolling the GMRF model).

This shows the PGM-like flexibility of QT, answering queries on blocks that it was never trained for. Of course, large departures from the statistics of the training queries can result in poor predictions.

3.2 Grid Markov random field (GMRF)

We consider the challenging problem of using QT to learn an 8-connected, grid-arranged Markov random field (MRF) *with hidden variables*, as shown in Fig. 2b. Although the models explored so far also had hidden variables, they did not have direct connections—as it is the case now—which make the model more loopy and learning more challenging. Grid MRFs are often used in image processing applications [Li, 2009], but the MRF variables are always observed when learning the factor parameters. In our case, the MRF variables are hidden, and they emit the pixel labels through a noisy channel, with multiple hidden states mapping to the same pixel labels.

To the best of our knowledge, QT is the first method that can learn the full parameterization of an 8-connected grid MRF without access to the MRF variables. Although irrelevant for our purpose of learning a challenging undirected PGM, the proposed model is a simple incarnation of visual neuroscience principles for foreground–background segmentation. Further details about the model and its neuroscience motivation are presented in the Supplementary Material.

3.2.1 The border ownership dataset, model, and task

The border ownership dataset is provided with the Supplementary Material and is derived from the MNIST dataset⁸ [LeCun et al., 2010]. It is structured as pairs of noisy contour images and CONTOUR-IN-OUT labels. Two examples are displayed in Fig. 2c. The contours are missing with probability 0.2, whereas each image incorporates 8 spurious random edges of length 3 pixels. Each image is of size 30×30 pixels. The images have one-to-one correspondence with the MNIST dataset, so 60,000 images are available for training and 10,000 images are used for testing.

The structure of the MRF is shown in Fig. 2b. Each node is a categorical variable with 66 hidden states, 64 correspond to the label CONTOUR, 1 to IN, and 1 to OUT. The vertical connections are a noisy channel. There are only 4 distinct pairwise factors (different colors in Fig. 2b). The task is to recover the hidden labels from the noisy image. Observe that the incomplete contours and the spurious edges make the task of foreground–background segmentation non-trivial. Second, observe that the labels do *not* provide the hidden states. In particular, which of the 64 clones of CONTOUR is appropriate for each pixel is unknown, and the use of multiple clones is required to properly solve the task, since the potentials are only local pairwise connections and long-range information is needed.

3.2.2 Results

The model is trained using QT. The input and output variables in this case are not randomized, but fixed throughout training and testing: the evidence is always the noisy binary image and the target is always the noiseless ternary segmentation. We unroll BP for $N = 15$ layers, use ADAM with a learning rate of 10^{-2} with minibatches of 50 images and run learning for 10 epochs on a single Tesla V100 GPU. The temperature parameter is fixed $T = 1$ throughout learning. The results of segmentation from noisy test data are shown on Fig. 2d for several example digits. Pixels decoded as CONTOUR, IN, OUT are respectively in red, pale blue, and pale yellow. Qualitatively, the recovery looks almost perfect. Quantitatively, Table 2 presents the intersection over union (IoU) between the estimated and real foreground⁹, and the NCE of a GMRF trained with QT and with a random baseline. QT achieves a nearly perfect digit recovery.

Table 2: Results for QT and a random baseline for GMRF on the test border ownership dataset.

Method	IOU	NCE
QT (OURS)	96.97	0.0398
RANDOM	16.39	1.00

We have tried to train the GMRF using other alternatives without luck. In particular, AdVIL requires designing three new encoder networks and one decoder network for this model. Our network designs have failed to produce any meaningful results in a reasonable amount of time.

4 Discussion and future work

Query training is a general approach to learn to infer when the inference target is unknown at training time. It offers the following advantages: (a) a systematic approach to convert any PGM, even with hidden variables, into an inference network that supports novel queries (see Section 3.1.3); (b) no need to estimate the partition function (the “sleep” phase), so particularly applicable to undirected PGMs; (c) a simple learning and inference mechanism built in (e.g., AdVIL needed Gibbs sampling to answer our queries); (d) learning can correct for BP inaccuracies or too few inference steps, potentially making QT-NN faster and/or more accurate than BP itself.

Why would QT generalize to new queries or scale well? The worry is that only a small fraction of the exponential number of potential queries is seen during training. The *existence* of a single inference network that works well for many different queries follows from the existence of a single PGM in which BP can approximate inference. The *discoverability* of such a network from limited training

⁸The MNIST dataset can be found at <http://yann.lecun.com/exdb/mnist/>.

⁹For the purpose of this metric, we consider foreground those pixels labeled (or estimated) as either IN, CONTOUR. Higher is better.

data is not guaranteed. However, there is hope for it, since the amount of training data required to adjust the model parameters should scale with the number of these, and not with the number of potential queries. Just like training data should come from the same distribution as test data, the training queries must come from the same distribution as the test queries to avoid “query overfitting”.

Interesting avenues for exploration are model sampling and other inference mechanisms, such as VI.

Broader Impact

Developing efficient learning mechanisms for undirected graphical models results in a) a larger breadth of PGMs being available to model a given phenomenon or machine learning problem, which in turn produces b) superior results when undirected graphical models are more suitable. This can result in superior performance of AI systems, reduced training times, reduced computing costs, and reduced environmental pollution. As with any technology, negative consequences are possible but difficult to predict at this time. This is not a deployed system with immediate failure consequences or that can by itself leverage harmful biases, although these are possible when integrated into more complex systems.

References

- M. Abadi, A. Agarwal, P. Barham, E. Brevdo, Z. Chen, C. Citro, G. S. Corrado, A. Davis, J. Dean, M. Devin, S. Ghemawat, I. Goodfellow, A. Harp, G. Irving, M. Isard, Y. Jia, R. Jozefowicz, L. Kaiser, M. Kudlur, J. Levenberg, D. Mané, R. Monga, S. Moore, D. Murray, C. Olah, M. Schuster, J. Shlens, B. Steiner, I. Sutskever, K. Talwar, P. Tucker, V. Vanhoucke, V. Vasudevan, F. Viégas, O. Vinyals, P. Warden, M. Wattenberg, M. Wicke, Y. Yu, and X. Zheng. TensorFlow: Large-scale machine learning on heterogeneous systems, 2015. URL <https://www.tensorflow.org/>. Software available from tensorflow.org.
- J. Besag. Statistical analysis of non-lattice data. *Journal of the Royal Statistical Society: Series D (The Statistician)*, 24(3):179–195, 1975.
- D. M. Blei, A. Kucukelbir, and J. D. McAuliffe. Variational inference: A review for statisticians. *Journal of the American statistical Association*, 112(518):859–877, 2017.
- J. K. Bradley. *Learning Large-Scale Conditional Random Fields*. PhD thesis, Intel, 2013.
- G. V. Cormack and R. N. S. Horspool. Data compression using dynamic Markov modelling. *The Computer Journal*, 30(6):541–550, 1987.
- J. Hawkins, D. George, and J. Niemasik. Sequence memory for prediction, inference and behaviour. *Philosophical Transactions of the Royal Society B: Biological Sciences*, 364(1521):1203–1209, 2009.
- G. E. Hinton. Training products of experts by minimizing contrastive divergence. *Neural computation*, 14(8):1771–1800, 2002.
- A. Hyvärinen. Consistency of pseudolikelihood estimation of fully visible boltzmann machines. *Neural Computation*, 18(10):2283–2292, 2006.
- D. P. Kingma and J. Ba. Adam: A method for stochastic optimization. *arXiv preprint arXiv:1412.6980*, 2014.
- D. P. Kingma and M. Welling. Auto-encoding variational bayes. *arXiv preprint arXiv:1312.6114*, 2013.
- V. Kuleshov and S. Ermon. Neural variational inference and learning in undirected graphical models. In *Advances in Neural Information Processing Systems*, pages 6734–6743, 2017.
- Y. LeCun, C. Cortes, and C. Burges. Mnist handwritten digit database, 2010.
- C. Li, C. Du, K. Xu, M. Welling, J. Zhu, and B. Zhang. To relieve your headache of training an MRF, take AdVIL. *arXiv preprint arXiv:1901.08400*, 2019.

- S. Z. Li. *Markov random field modeling in image analysis*. Springer Science & Business Media, 2009.
- B. Marlin, K. Swersky, B. Chen, and N. Freitas. Inductive principles for restricted Boltzmann machine learning. In *Proceedings of the Thirteenth International Conference on Artificial Intelligence and Statistics*, pages 509–516, 2010.
- T. P. Minka. Expectation propagation for approximate bayesian inference. In *Proceedings of the Seventeenth conference on Uncertainty in artificial intelligence*, pages 362–369, 2001.
- K. Murphy, Y. Weiss, and M. I. Jordan. Loopy belief propagation for approximate inference: An empirical study. *arXiv preprint arXiv:1301.6725*, 2013.
- P. O’Herron and R. von der Heydt. Short-term memory for figure-ground organization in the visual cortex. *Neuron*, 61(5):801–809, 2009.
- P. O’Herron and R. von der Heydt. Remapping of border ownership in the visual cortex. *Journal of Neuroscience*, 33(5):1964–1974, 2013.
- A. Paszke, S. Gross, F. Massa, A. Lerer, J. Bradbury, G. Chanan, T. Killeen, Z. Lin, N. Gimelshein, L. Antiga, et al. Pytorch: An imperative style, high-performance deep learning library. In *Advances in Neural Information Processing Systems*, pages 8024–8035, 2019.
- F. Pedregosa, G. Varoquaux, A. Gramfort, V. Michel, B. Thirion, O. Grisel, M. Blondel, P. Prettenhofer, R. Weiss, V. Dubourg, J. Vanderplas, A. Passos, D. Cournapeau, M. Brucher, M. Perrot, and E. Duchesnay. Scikit-learn: Machine learning in Python. *Journal of Machine Learning Research*, 12:2825–2830, 2011.
- D. J. Rezende, S. Mohamed, and D. Wierstra. Stochastic backpropagation and approximate inference in deep generative models. *arXiv preprint arXiv:1401.4082*, 2014.
- C. Sutton and A. McCallum. Piecewise training for undirected models. In *Proceedings of the Twenty-First Conference on Uncertainty in Artificial Intelligence*, pages 568–575. AUAI Press, 2005.
- C. Sutton and A. McCallum. Piecewise pseudolikelihood for efficient training of conditional random fields. In *Proceedings of the 24th international conference on Machine learning*, pages 863–870. ACM, 2007.
- C. Sutton and T. Minka. Local training and belief propagation. Technical report, Technical Report TR-2006-121, Microsoft Research, 2006.
- T. Tieleman. Training restricted boltzmann machines using approximations to the likelihood gradient. In *Proceedings of the 25th international conference on Machine learning*, pages 1064–1071. ACM, 2008.
- M. Titsias and M. Lázaro-Gredilla. Doubly stochastic variational bayes for non-conjugate inference. In *International conference on machine learning*, pages 1971–1979, 2014.
- A. Van Oord, N. Kalchbrenner, and K. Kavukcuoglu. Pixel recurrent neural networks. In *International Conference on Machine Learning*, pages 1747–1756, 2016.
- M. Welling and C. A. Sutton. Learning in Markov random fields with contrastive free energies. In *AISTATS*, 2005.
- J. Xu, T. L. Wickramaratne, and N. V. Chawla. Representing higher-order dependencies in networks. *Science advances*, 2(5):e1600028, 2016.
- L. Zhaoping. Border ownership from intracortical interactions in visual area v2. *Neuron*, 47(1): 143–153, 2005.
- H. Zhou, H. S. Friedman, and R. Von Der Heydt. Coding of border ownership in monkey visual cortex. *Journal of Neuroscience*, 20(17):6594–6611, 2000.

Appendices

A Hidden activations learned by the 8-connected GMRF



Figure 3: Best viewed on screen with zoom. Each color corresponds to a different inferred hidden contour clone. The model has learned *with no supervision* to capture the local orientation of the pixel (which also reveals on which side the foreground is) as the best way to solve the denoising task.

B Visual neuroscience and model details for the GMRF

The purpose of this model is to perform some rudimentary foreground–background segmentation from noisy cues of the edges of the foreground, see Fig. 4. There is abundant literature supporting border ownership as mechanism for foreground–background segmentation [O’Herron and von der Heydt, 2009, 2013, Zhaoping, 2005, Zhou et al., 2000], and the use of “clones” for representing higher-order dependencies [Hawkins et al., 2009, Xu et al., 2016, Cormack and Horspool, 1987]. A simplified model based on these principles is presented in Fig. 5. It has two types of variables, pixel labels (white, hidden, categorical with 66 categories) and pixel intensities (gray, observed, binary). The pixel labels categorize a pixel as belonging to the OUT (one category), IN (one category), or CONTOUR (64 distinct categories) of the foreground surface. In the noiseless case, the emission factors (vertical) are deterministic: the IN and OUT pixel labels produce pixel intensity 0, whereas the 64 remaining categories (CONTOUR) produce pixel intensities 1. The point of having 64 apparently identical categories, all of which generate a contour (these are the “clones”), is that those hidden labels can specialize and learn higher order properties of the contour, such as its orientation and the side of the foreground on which they are located. Thus, a pixel that is part of a horizontal contour will

have a different pixel label than another pixel that is part of a vertical contour. Now, a CONTOUR pixel whose hidden label is “bottom horizontal” is likely to turn on other “bottom horizontal” pixels on its left and right and IN pixels on top of it. This allows to represent the long-range interactions required for foreground–background segmentation using only pairwise factors. Note that these labels are just a possible specialization that training can discover, these are not available! The system contains unsupervised hidden variables. Due to its arrangement on a grid, we call this model the grid MRF (GMRF).

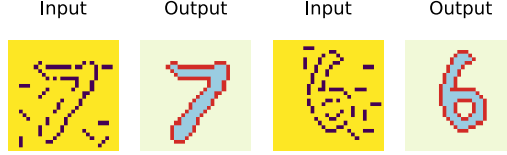


Figure 4: Two examples of training pairs: a noisy input digit and its corresponding ground truth segmentation

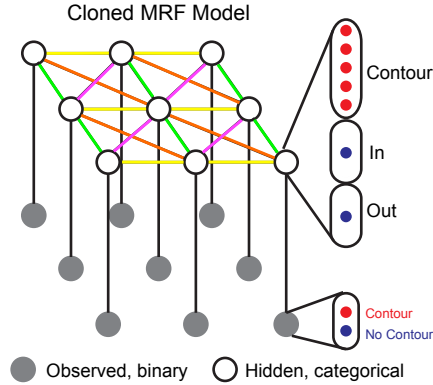


Figure 5: An 8-connected grid Markov random field. Identical factors are shown using the same color. Actual size, 30×30 .

Model details: First, let us consider the lateral connections between pixel labels in Fig. 5. The model is fully convolutional, meaning that there are only 4 different types of potentials: up-down (green), left-right (yellow), principal diagonal (orange) and secondary diagonal (purple). These are color-coded in Fig. 5, and extend in every direction to accommodate any GMRF size. This means that the model will perform the same segmentation regardless of where in the image the surface is presented (barring edge effects). These factors connect pairs of categorical variables with 66 values, are fully parametric, and are learned by QT.

The vertical connections (emission factors) are either known a priori or easy to estimate, so they are fixed during QT learning. In the noiseless case, they deterministically map to 0 or 1 as described above. In the noisy case, we have 3 noise parameters that determine the probability of generating a 1 conditioned on the label type being CONTOUR, IN or OUT. If we have access to ground truth segmentations and noisy images (as it is the case in our training data), those 3 parameters can be estimated in closed form.

To handle segmentation from noisy images, it is useful to think of this model as having both the noisy emission factors (producing the noisy image) and noiseless emissions factors that emit the segmentation categories: CONTOUR, IN and OUT. We will condition on the first and target the second.

Table 3: Standard deviation of the mean for RBM results in the main paper

Method	Adult	Conn4	Digits	DNA	Mushr	NIPS	OCR	RCV1	Web
AdVIL-BP	4.55×10^{-4}	7.44×10^{-5}	1.66×10^{-3}	2.22×10^{-5}	4.36×10^{-4}	7.9×10^{-4}	2.83×10^{-3}	1.48×10^{-4}	2.29×10^{-4}
AdVIL-Gibbs	7.84×10^{-4}	4.98×10^{-3}	1.29×10^{-3}	8.71×10^{-4}	4.06×10^{-3}	6.77×10^{-4}	8.55×10^{-4}	1.13×10^{-4}	7.32×10^{-3}
PCD-BP	1.52×10^{-3}	2.88×10^{-3}	1.18×10^{-3}	6.86×10^{-4}	2.74×10^{-3}	2.48×10^{-3}	9.78×10^{-4}	1.85×10^{-4}	1.56×10^{-4}
PCD-Gibbs	1.86×10^{-3}	2.58×10^{-3}	8.09×10^{-4}	9.68×10^{-4}	3.2×10^{-3}	2.07×10^{-3}	1.28×10^{-3}	1.94×10^{-4}	2.24×10^{-4}
QT (Ours)	3.26×10^{-4}	7.34×10^{-4}	5.77×10^{-4}	8.45×10^{-4}	1.68×10^{-3}	6.37×10^{-5}	1.09×10^{-3}	3.06×10^{-4}	2.06×10^{-4}

C Details of experimental results

C.1 Restricted Boltzmann machine (RBM)

C.2 Deep Boltzmann machine (DBM)

Table 4: Standard deviation of the mean for DBM results in the main paper

Method	Adult	Conn4	Digits	DNA	Mushr	NIPS	OCR	RCV1	Web
AdVIL-BP	2.56×10^{-4}	1.81×10^{-4}	1.03×10^{-3}	7×10^{-4}	5.89×10^{-4}	2.98×10^{-4}	4.05×10^{-4}	1.02×10^{-4}	1.01×10^{-4}
AdVIL-Gibbs	1.27×10^{-4}	1.08×10^{-4}	1.03×10^{-3}	3.75×10^{-4}	1.61×10^{-3}	3.93×10^{-4}	6.28×10^{-4}	1.30×10^{-4}	1.94×10^{-4}
QT (Ours)	1.21×10^{-3}	5.17×10^{-4}	2.82×10^{-4}	2.53×10^{-4}	4.29×10^{-4}	4.27×10^{-4}	6.96×10^{-4}	2.21×10^{-4}	7.74×10^{-5}

C.3 Gaussian restricted Boltzmann machine (GRBM)

Table 5: Standard deviation of the mean for GRBM results in the main paper

Method	Exp. 1	Exp. 2
AdVIL-Gibbs	9.31×10^{-5}	1.08×10^{-3}
AdVIL-BP	1.91×10^{-5}	2.58×10^{-3}
QT (Ours)	8.64×10^{-4}	1.06×10^{-3}

C.4 Grid Markov random field (GMRF)

Table 6: Standard deviation of the mean for GMRF results in the main paper. The RANDOM approach is fully deterministic, so there is no difference in results between independent runs.

Method	IOU	NCE
QT (OURS)	0.28	0.34
RANDOM	9.0×10^{-3}	0

D QT-NN architectures, derived for each PGM class

Here we derive efficient and numerically robust forms of the BP update equations for each of our models. These form the QT-NNs used and trained in the main paper.

D.1 Restricted Boltzmann machine (RBM)

RBM potential: We consider the case where the underlying PGM is a binary RBM with H hidden units and V visible units. We will use a slightly different parameterization (a linear transformation of the standard one) to simplify the form of the obtained transfer function. Thus, we set

$$\phi(\mathbf{v}, \mathbf{h}; \theta) = 2\mathbf{h}^\top \mathbf{W} \mathbf{v} + \mathbf{h}^\top (\mathbf{c}_H - \mathbf{W} \mathbf{1}_V) + \mathbf{v}^\top (\mathbf{c}_V - \mathbf{W}^\top \mathbf{1}_H) \quad (2)$$

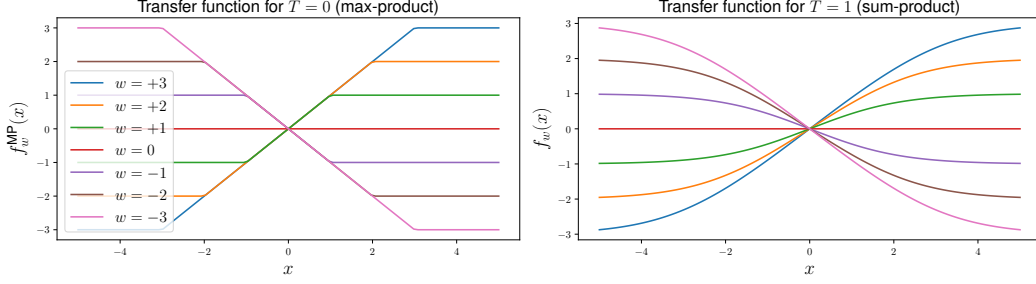


Figure 6: Transfer function for binary pairwise factors (with score 0 for agreement and $-w$ for disagreement) at two temperatures, max-product and sum-product. With this parameterization, setting a weight or input to zero results in zero output.

Note that the above potential can be expressed as:

$$\begin{aligned} \phi(\mathbf{v}, \mathbf{h}; \theta) = & \frac{1}{2}(\mathbf{2h} - \mathbf{1}_H)^\top W(\mathbf{2v} - \mathbf{1}_V) + \frac{1}{2}(\mathbf{2h} - \mathbf{1}_H)^\top \mathbf{c}_H + \frac{1}{2}(\mathbf{2v} - \mathbf{1}_V)^\top \mathbf{c}_V \\ & - \frac{1}{2}\mathbf{1}_H^\top W \mathbf{1}_V + \frac{1}{2}\mathbf{c}_H^\top \mathbf{1}_H + \frac{1}{2}\mathbf{c}_V^\top \mathbf{1}_V. \end{aligned}$$

We can therefore define $\tilde{\mathbf{h}} = \mathbf{2h} - \mathbf{1}_H$; $\tilde{\mathbf{v}} = \mathbf{2v} - \mathbf{1}_V$ and consider the binary RBM where the hidden and visible variables take their values in $\{-1, 1\}$ and which has the potential:

$$\tilde{\phi}(\tilde{\mathbf{v}}, \tilde{\mathbf{h}}; \theta) = \frac{1}{2}\tilde{\mathbf{h}}^\top W \tilde{\mathbf{v}} + \frac{1}{2}\tilde{\mathbf{h}}^\top \mathbf{c}_H + \frac{1}{2}\tilde{\mathbf{v}}^\top \mathbf{c}_V.$$

ϕ and $\tilde{\phi}$ only differ by a constant of the model parameters, which will be cancelled out by the partition function. The RBM models are therefore equivalent. Three kinds of potentials are involved in $\tilde{\phi}$:

- potentials between hidden and visible variables: $\psi_{ij}(\tilde{h}_i, \tilde{v}_j) = \exp\left(\frac{1}{2} w_{ij} \tilde{h}_i \tilde{v}_j\right)$, $\forall i, j$.
- potentials associated with hidden variables: $\kappa_i(\tilde{h}_i) = \exp\left(\frac{1}{2} c_{H,i} \tilde{h}_i\right)$, $\forall i$.
- potentials associated with visible variables: $\theta_j(\tilde{v}_j) = \exp\left(\frac{1}{2} c_{V,j} \tilde{v}_j\right)$, $\forall j$.

BP updates: We denote $N_{HV} \in \mathbb{R}_+^{H \times V \times 2}$ (resp. $N_{VH} \in \mathbb{R}_+^{V \times H \times 2}$) the messages going from the visible variables to the hidden variables (resp. from the hidden variables to the visible variables).

For an observed vector $\mathbf{x} \in \{-1, 1\}^V$ and a query vector $\mathbf{q} \in \{0, 1\}^V$, we note $\phi(v_i, x_i)$ the bottom-up messages to the i th visible variable. We have $\phi(-1, x_i) = \phi(1, x_i) = 0.5$ if x_i is being queried ($q_i = 0$); and $\phi(v_i, x_i) = 1$ if $v_i = x_i$ and 0 otherwise if x_i is being observed ($q_i = 1$). It therefore holds: $\phi(-1, x_i) + \phi(1, x_i) = 1$. All hidden variables are considered as being queried.

For the sake of simplicity, we first derive the BP updates for the sum-product BP algorithm with parallel schedules, before generalizing to a general temperature T . The message going from the j th visible variables to the i th hidden variables can be expressed as

$$n_{HV}^{ij}(\tilde{h}_j) \propto \sum_{\tilde{v}_j \in \{-1, 1\}} \psi_{ij}(\tilde{h}_i, \tilde{v}_j) \phi(\tilde{v}_j, x_j) \theta_j(\tilde{v}_j) \prod_{k \neq i} n_{VH}^{jk}(\tilde{v}_j), \quad \forall \tilde{h}_i \in \{-1, 1\}, \quad (3)$$

which is equivalent to

$$\begin{aligned} n_{HV}^{ij}(\tilde{h}_i) \propto & \psi_{ij}(\tilde{h}_i, -1) \phi(-1, x_j) \theta_j(-1) \prod_{k \neq i} n_{VH}^{jk}(-1) \\ & + \psi_{ij}(\tilde{h}_i, 1) \phi(1, x_j) \theta_j(1) \prod_{k \neq i} n_{VH}^{jk}(1), \quad \forall \tilde{h}_i \in \{-1, 1\} \end{aligned} \quad (4)$$

The BP updates for messages going from the hidden variables to the visible ones can be expressed in a similar fashion.

Numerical stability can be encouraged with the two following steps. First, we normalize messages:

$$n_{HV}^{ij}(1) + n_{HV}^{ij}(-1) = 1.$$

Second, we map the messages to the logit space. Messages can then be expressed by a single float. We denote $M_{HV} \in \mathbb{R}^{H \times V}$ and $M_{VH} \in \mathbb{R}^{V \times H}$ the messages in the logit space. The sum-product BP updates in Equation (4) are equivalent to:

$$\begin{aligned} m_{HV}^{ij} &= \text{logit} \left(n_{HV}^{ij}(1) \right) = \log \left(n_{HV}^{ij}(1) \right) - \log \left(1 - n_{HV}^{ij}(1) \right) \\ &= \log \left(n_{HV}^{ij}(1) \right) - \log \left(n_{HV}^{ij}(-1) \right) \\ &= \log \left(\psi_{ij}(1, -1) \phi(-1, x_j) \theta_j(-1) \prod_{k \neq i} n_{VH}^{jk}(-1) + \psi_{ij}(1, 1) \phi(1, x_j) \theta_j(1) \prod_{k \neq i} n_{VH}^{jk}(1) \right) \\ &\quad - \log \left(\psi_{ij}(-1, -1) \phi(-1, x_j) \theta_j(-1) \prod_{k \neq i} n_{VH}^{jk}(-1) + \psi_{ij}(-1, 1) \phi(1, x_j) \theta_j(1) \prod_{k \neq i} n_{VH}^{jk}(1) \right) \\ &= \log \left(\psi_{ij}(1, -1) \phi(-1, x_j) \theta_j(-1) + \psi_{ji}(1, 1) \phi(1, x_j) \theta_j(1) \prod_{k \neq i} \exp \left(m_{VH}^{jk} \right) \right) \\ &\quad - \log \left(\psi_{ij}(-1, -1) \phi(-1, x_j) \theta_j(-1) + \psi_{ij}(-1, 1) \phi(1, x_j) \theta_j(1) \prod_{k \neq i} \exp \left(m_{VH}^{jk} \right) \right) \\ &= \log \left(1 + \frac{\psi_{ij}(1, 1) \phi(1, x_j) \theta_j(1)}{\psi_{ij}(1, -1) \phi(-1, x_j) \theta_j(-1)} \prod_{k \neq i} \exp \left(m_{VH}^{jk} \right) \right) + \log \left(\psi_{ji}(1, -1) \phi(-1, x_j) \theta_j(-1) \right) \\ &\quad - \log \left(1 + \frac{\psi_{ij}(-1, 1) \phi(1, x_j) \theta_j(1)}{\psi_{ij}(-1, -1) \phi(-1, x_j) \theta_j(-1)} \prod_{k \neq i} \exp \left(m_{VH}^{jk} \right) \right) - \log \left(\psi_{ij}(-1, -1) \phi(-1, x_j) \theta_j(-1) \right) \\ &= \log \left(1 + \exp \left\{ w_{ij} + u_j + c_{V,j} + \sum_{k \neq i} m_{VH}^{jk} \right\} \right) - \log \left(1 + \exp \left\{ -w_{ij} + u_j + c_{V,j} + \sum_{k \neq i} m_{VH}^{jk} \right\} \right) \\ &\quad - w_{ij} \\ &= f_{w_{ij}} \left(u_j + c_{V,j} + \sum_{k \neq i} m_{VH}^{jk} \right), \end{aligned}$$

where we have defined $f_w(x) = \log(1 + e^{x+w}) - \log(1 + e^{x-w}) - w$ and $u_j = \text{logit} \phi(1, x_j)$ ¹⁰.

Note that we can simply express $u_j = \text{logit} \left(\frac{1+x_j}{2} \right) q_j$.

For numerical stability of the message updates, we use the property:

$$\begin{aligned} f_w(x) &= \log(1 + e^{x+w}) - \log(1 + e^{x-w}) - w = \log(1 + e^{x+w}) - \log(e^w + e^x) \\ &= \text{sign}(w) x \frac{|w|}{|w|} + \log(1 + e^{-|x+w|}) - \log(1 + e^{-|x-w|}). \end{aligned}$$

After running the BP updates for N iterations, we compute the beliefs (in the logit space) for the j th visible variable

$$\begin{aligned} b_{V,j} &= \log \left(\phi(1, x_j) \theta_j(1) \prod_{k=1}^H n_{VH}^{jk}(1) \right) - \log \left(\phi(-1, x_j) \theta_j(-1) \prod_{k=1}^H n_{VH}^{jk}(-1) \right) \\ &= u_j + c_{V,j} + \sum_{k=1}^H m_{VH}^{jk}, \end{aligned}$$

and map the beliefs back to the real space by considering the sigmoid of this quantity.

¹⁰In practice we clip the messages so that $u_i = -1000, 0, 1000$ for the values $\phi(1, x_j) = 0, 0.5, 1$.

BP summary: We can summarize the architecture of the QT-NN for a general temperature T by the following equations (which correspond to the unrollment of parallel BP over time using messages in logit space presented above):

$$\begin{aligned}
\mathbf{u}_V &= \text{logit} \left(\frac{\mathbf{x} + 1}{2} \right) \circ \mathbf{q} && \text{(unary term for visible units)} \\
\mathbf{u}_H &= \mathbf{0}_H && \text{(unary term for hidden units)} \\
M_{HV}^{(0)} &= \mathbf{0}_{HV} && \text{(init messages to 0)} \\
M_{VH}^{(0)} &= \mathbf{0}_{VH} && \text{(init messages to 0)} \\
M_{HV}^{(n)} &= f_{W^\top} \left(\mathbf{u}_V \mathbf{1}_H^T + \mathbf{c}_V \mathbf{1}_H^T + M_{VH}^{(n-1)} \mathbf{1}_{HH} - M_{VH}^{(n-1)} \right)^\top && \text{(interlayer connection)} \\
M_{VH}^{(n)} &= f_W \left(\mathbf{u}_H \mathbf{1}_V^T + \mathbf{c}_H \mathbf{1}_V^T + M_{HV}^{(n-1)} \mathbf{1}_{VV} - M_{HV}^{(n-1)} \right)^\top && \text{(interlayer connection)} \\
\hat{\mathbf{v}} &= \sigma \left(\mathbf{u}_V + \mathbf{c}_V + M_{VH}^{(N)} \mathbf{1}_H \right) && \text{(output layer for visible)} \\
\hat{\mathbf{h}} &= \sigma \left(\mathbf{u}_H + \mathbf{c}_H + M_{HV}^{(N)} \mathbf{1}_V \right) && \text{(output layer for hidden),}
\end{aligned}$$

where

$$\begin{aligned}
\sigma(x) &= 1/(1 + e^{-x}) \\
\text{logit}(x) &= \sigma^{-1}(x) = \log(x) - \log(1 - x) \\
f_w^{\text{MP}}(x) &= \text{sign}(w)x^{|w|}_{-|w|} && (a|_b^c \text{ truncates } a \text{ between } b \text{ and } c, \text{ Fig. 6 left}) \\
f_w(x) &= f_w^{\text{MP}}(x) + \text{sp}(-|x + w|, T) - \text{sp}(-|x - w|, T) && \text{(Fig. 6 right)} \\
\text{sp}(x, T) &= T \log(1 + e^{x/T}) && \text{(a.k.a. softplus function).}
\end{aligned}$$

We have used the following notations:

- $\mathbf{0}_{HV}$ represents a matrix of zeros of size $H \times V$. Similarly $\mathbf{1}_{HH}$ represents a matrix of ones of size $H \times H$, and $\mathbf{1}_V$ represents a matrix of ones of size $V \times 1$.
- When any of the above defined scalar functions is used with matrix arguments, the function is applied elementwise.

Some observations can be made:

- The Hadamard product with \mathbf{q} effectively removes the information from the elements of \mathbf{v} not present in the query mask, replacing them with 0, which corresponds to a uniform binary distribution in logit space.
- The output of the network is $\hat{\mathbf{v}}$ and $\hat{\mathbf{h}}$, the inferred probability of 1 for both the visible and hidden units. The output $\hat{\mathbf{h}}$ is inferred but actually not used during training.
- The computation of $f_w(x)$ as specified above is designed to be numerically robust. It starts by computing $f_w^{\text{MP}}(x)$, which would be the value of $f_w(x)$ for a temperature $T = 0$, i.e., max-product message passing, and then performs a correction on top for positive temperatures.

D.2 Deep Boltzmann machine (DBM)

In this section we consider the slightly more complicated case in which the underlying PGM is a binary DBM with V visible units and two hidden layers with H_1 and H_2 units. As in Section D.1, we use the slightly different parametrization

$$\begin{aligned}
&\phi(\mathbf{v}, \mathbf{h}; \theta) \\
&= 2\mathbf{h}_2^\top W_{H_2 H_1} \mathbf{h}_1 + 2\mathbf{h}_1^\top W_{H_1 V} \mathbf{v} + \mathbf{h}_2^\top (\mathbf{c}_{H_2} - W_{H_2 H_1} \mathbf{1}_{H_1}) + \mathbf{v}^\top (\mathbf{c}_V - W_{H_1 V}^\top \mathbf{1}_{H_1}) \\
&+ \mathbf{h}_1^\top (\mathbf{c}_{H_1} - W_{H_2 H_1}^\top \mathbf{1}_{H_2} - W_{H_1 V} \mathbf{1}_V)
\end{aligned} \tag{5}$$

We note that, due to the fact that we are considering a DBM with just two hidden layers, we can reuse the equations derived in Section D.1 by some simple transformations. More concretely, define

$$\tilde{\mathbf{h}} = \mathbf{h}_1, \tilde{\mathbf{v}} = \begin{bmatrix} \mathbf{v} \\ \mathbf{h}_2 \end{bmatrix}, \tilde{W} = \begin{bmatrix} W_{H_1V} \\ W_{H_2H_1}^\top \end{bmatrix}, \tilde{\mathbf{c}}_H = \mathbf{c}_{H_1}, \tilde{\mathbf{c}}_V = \begin{bmatrix} \mathbf{c}_V \\ \mathbf{c}_{H_2} \end{bmatrix}$$

It's easy to see that plugging $\tilde{\mathbf{h}}, \tilde{\mathbf{v}}, \tilde{W}, \tilde{\mathbf{c}}_H, \tilde{\mathbf{c}}_V$ into Equation 2 recovers Equation 5.

As a result, the QT-NN equations derived in Section D.1 for the RBM apply equally well to the DBM with two hidden layers. The only change needed lies in the incoming messages and the queries. Use v, q to denote the original observed values for the visible units and our interested query. The corresponding unary term for visible units for DBM is define as $\mathbf{u}_V = \text{logit}(\tilde{\mathbf{v}}) \circ \tilde{\mathbf{q}}$, where

$$\tilde{\mathbf{v}} = \begin{bmatrix} \mathbf{v} \\ 0.5\mathbf{1}_{H_2} \end{bmatrix} \text{ and } \tilde{\mathbf{q}} = \begin{bmatrix} \mathbf{q} \\ \mathbf{1}_{H_2} \end{bmatrix}$$

D.3 Gaussian restricted Boltzmann machine (GRBM)

The log-probability of a GRBM is proportional to:

$$\phi(\mathbf{v}, \mathbf{h}; \theta) = -\frac{1}{2\sigma^2} \|\mathbf{v} - \mathbf{b}\|^2 + \mathbf{c}^\top \mathbf{h} + \frac{1}{\sigma} \mathbf{h}^\top W \mathbf{v} \quad (6)$$

where σ is fixed to 1. To embed passing of continuous messages in the QT-NN, we approximate continuous messages with Gaussian distributions. In the following equations, for every message to a visible unit, we store the two natural parameters of a Gaussian distribution corresponding to that message.

$$\begin{aligned} \mathbf{u}_H &= \mathbf{0}_H && \text{(unary term for hidden units)} \\ \mathbf{u}_{V\theta_1} &= \mathbf{v} \circ \mathbf{q} + \mathbf{b} \circ (\mathbf{1}_V - \mathbf{q}) && \text{(param 1 for visible unary term)} \\ \mathbf{u}_{V\theta_2} &= -\frac{1}{2\epsilon} \cdot \mathbf{q} - \frac{1}{2} \cdot (\mathbf{1}_V - \mathbf{q}) && \text{(param 2 of visible unary term)} \\ M_{HV}^{(0)} &= \mathbf{0}_{HV} && \text{(init message from visible to hidden)} \\ M_{VH\theta_1}^{(0)} &= \mathbf{0}_{VH} && \text{(init message from hidden to visible)} \\ M_{VH\theta_2}^{(0)} &= -\frac{1}{2} \cdot \mathbf{1}_{VH} && \text{(init message from hidden to visible)} \\ C_{VH\theta_1}^{(n-1)} &= \mathbf{u}_{V\theta_1} + M_{VH\theta_1}^{(n-1)} \mathbf{1}_H - M_{VH\theta_1}^{(n-1)} && \text{(param 1 of cavity)} \\ C_{VH\theta_2}^{(n-1)} &= \mathbf{u}_{V\theta_2} + M_{VH\theta_2}^{(n-1)} \mathbf{1}_H - M_{VH\theta_2}^{(n-1)} && \text{(param 2 of cavity)} \\ M_{HV}^{(n)} &= f_{W^\top}(C_{VH\theta_1}^{(n-1)}, C_{VH\theta_2}^{(n-1)})^\top && \text{(interlayer connection)} \\ C_{HV}^{(n-1)} &= \mathbf{u}_H + \mathbf{c}_H + M_{HV}^{(n-1)} \mathbf{1}_V - M_{HV}^{(n-1)} && \text{(cavity)} \\ M_{VH\theta_1}^{(n)}, M_{VH\theta_2}^{(n)} &= g_W(C_{HV}^{(n-1)}, C_{VH\theta_1}^{(n-1)}, C_{VH\theta_2}^{(n-1)}) && \text{(interlayer connection)} \\ \hat{\mathbf{v}}_{\theta_1} &= \mathbf{u}_{V\theta_1} + M_{VH\theta_1}^{(N)} \mathbf{1}_H && \text{(output layer for visible)} \\ \hat{\mathbf{v}}_{\theta_2} &= \mathbf{u}_{V\theta_2} + M_{VH\theta_2}^{(N)} \mathbf{1}_H && \text{(output layer for visible)} \\ \hat{\mathbf{h}} &= \sigma(\mathbf{u}_H + \mathbf{c}_H + M_{HV}^{(N)} \mathbf{1}_V) && \text{(output layer for hidden),} \end{aligned}$$

where

$$\begin{aligned} f_w(x, y) &= -\frac{2xw + w^2}{4y} \\ g_w(x, \theta_1, \theta_2) &= (b_1(w, x, \theta_1, \theta_2) - \theta_1, b_2(w, x, \theta_1, \theta_2) - \theta_2) \\ \sigma(x) &= 1/(1 + e^{-x}) \end{aligned}$$

Notation clarifications:

- θ_1 and θ_2 are used to denote the two natural parameters of a Gaussian distribution. In the case of $M_{VH\theta_1}$ and $M_{VH\theta_2}$, these are parameters approximating the messages from hidden units to visible units with a Gaussian distribution..
- The functions b_1 and b_2 output the two natural parameters of a Gaussian distribution approximating the belief at a visible unit, as is described below.

Given w (the weight of the connection between a hidden unit and visible unit), x (the cavity at the hidden unit), and θ_1, θ_2 (the natural parameters of the cavity at the visible unit), we approximate the belief at the visible unit as follows:

$$\begin{aligned}
\mu &= \frac{-\theta_1}{2\theta_2} \\
\sigma^2 &= \frac{-1}{2\theta_2} \\
\mu_B &= \frac{e^{x+w\mu+\frac{1}{2}\sigma^2w^2}(\mu+\sigma^2w)+\mu}{e^{x+w\mu+\frac{1}{2}\sigma^2w^2}+1} \\
\sigma_B^2 &= \frac{e^{x+w\mu+\frac{1}{2}\sigma^2w^2}((\mu+\sigma^2w)^2+\sigma^2)+\mu^2+\sigma^2}{e^{x+w\mu+\frac{1}{2}\sigma^2w^2}+1} - \mu_B^2
\end{aligned} \tag{7}$$

The approximation of the belief is a Gaussian with mean μ_B and variance σ_B^2 , and the functions b_1 and b_2 return the two natural parameters of that Gaussian, $\frac{\mu_B}{\sigma_B^2}$ and $-\frac{1}{\sigma_B^2}$ respectively.

E Statistical consistency

We discuss herein the appealing statistical properties of the query training estimator. In particular, we prove its local consistency for exponential family models.

Let d, n, m, K, L be integers. For a vector $\theta^* \in \mathbb{R}^d$, we consider an exponential family model with natural parameter θ^* and corresponding probability distribution function:

$$p(\mathbf{x}, \mathbf{z} | \theta^*) = \frac{1}{Z(\theta^*)} \exp((\theta^*)^T \mathbf{T}(\mathbf{x}, \mathbf{z})) = \frac{1}{Z(\theta^*)} \exp\left(\sum_{j=1}^d \theta_j^* T_j(\mathbf{x}, \mathbf{z})\right), \tag{8}$$

where $\mathbf{x} \in \{1, \dots, K\}^n$ is a vector of discrete observations, $\mathbf{z} \in \{1, \dots, L\}^m$ is a vector of discrete latent (unobserved) variables, and $\{T_j(\mathbf{x}, \mathbf{z})\}_{j=1}^d \in \mathbb{R}^d$ are sufficient statistics, that is, known functions of the data. $Z(\theta^*)$ is a normalising constant (the partition function), given by the sum:

$$Z(\theta^*) = \sum_{\mathbf{x} \in \{1, \dots, K\}^n, \mathbf{z} \in \{1, \dots, L\}^m} \exp\left(\sum_{j=1}^d \theta_j^* T_j(\mathbf{x}, \mathbf{z})\right),$$

which number of terms is exponential in the dimensions n and m .

We use query training (QT) to estimate θ^* from \mathbf{x} ; and we consider a uniform distribution over queries. For a natural parameter estimate $\theta \in \mathbb{R}^d$, the query associated with a non-empty subset $S \subset \{1, \dots, n\}$ is

$$Q_S(\theta) = \prod_{i \in S} p(x_i | \mathbf{x}_{-S}, \theta),$$

where \mathbf{x}_{-S} is the subset of observations with indexes outside S , and $p(\cdot | \theta)$ is defined as in Equation (8). Q_S is a random variable with respect to \mathbf{x} and S .

We consider the case of an infinite number of samples. A query training estimator is defined by

$$\hat{\theta} \in \operatorname{argmax}_{\theta \in \mathbb{R}^d} \bar{J}(\theta),$$

where the QT objective value considers the expectation over \mathbf{x} and S with respect to the exponential family pdf with natural parameter $\boldsymbol{\theta}^*$ (cf. Equation (8)) of the normalized logarithm of Q_S :

$$\bar{J}(\boldsymbol{\theta}) = \mathbb{E}_{\boldsymbol{\theta}^*} \left\{ \frac{1}{|S|} \log Q_S(\boldsymbol{\theta}) \right\} = \frac{1}{2^n - 1} \sum_{\substack{S \subset \{1, \dots, n\} \\ S \neq \emptyset}} \frac{1}{|S|} \sum_{i \in S} \mathbb{E}_{\boldsymbol{\theta}^*} \{ \log p(x_i | \mathbf{x}_{-S}, \boldsymbol{\theta}) \}. \quad (9)$$

If we only consider singleton queries, we obtain the pseudo-likelihood estimator, which is known to be consistent for fully visible Boltzman machines [Hyvärinen, 2006]. We generalize herein this result and show the local consistency of the query training estimator for exponential family models. The main steps are derived in Theorems 1 and 2.

Theorem 1 *The gradient of the QT objective value (defined in Equation (9)) evaluated for the ground truth natural parameter is equal to $\mathbf{0}$. That is, $\nabla_{\boldsymbol{\theta}} \bar{J}(\boldsymbol{\theta}^*) = \mathbf{0}$.*

We present the proof in Section E.1. In addition we prove in Section E.2 the following property:

Theorem 2 *The Hessian of the QT objective value evaluated for the ground truth natural parameter is negative semidefinite. That is, $\nabla_{\boldsymbol{\theta}}^2 \bar{J}(\boldsymbol{\theta}^*) \preceq 0$.*

We make the mild assumption that this Hessian is negative definite and conclude that in the case of an infinite amount of data, the QT estimator is equal to the ground truth $\boldsymbol{\theta}^*$ in a ball around $\boldsymbol{\theta}^*$.

Theorem 3 *Assume $\nabla_{\boldsymbol{\theta}}^2 \bar{J}(\boldsymbol{\theta}^*) \prec 0$. The query training estimator is locally consistent for the exponential family model defined in Equation (8).*

Proof of Theorem 3: By continuity, the Hessian of \bar{J} is negative definite in a compact ball around $\boldsymbol{\theta}^*$ and \bar{J} is strictly concave in this ball. In addition, $\boldsymbol{\theta}^*$ is a point of zero gradient. It is then the unique local maximizer of the objective value, and the QT estimator is locally consistent. \square

E.1 Proof of Theorem 1

Proof: For a natural parameter estimate $\boldsymbol{\theta} \in \mathbb{R}^d$, the query associated with a non-empty subset $S \subset \{1, \dots, n\}$ is

$$Q_S(\boldsymbol{\theta}) = \prod_{i \in S} Q_S^i(\boldsymbol{\theta}) = \prod_{i \in S} p(x_i | \mathbf{x}_{-S}, \boldsymbol{\theta}),$$

where we have noted $Q_S^i(\boldsymbol{\theta}) = p(x_i | \mathbf{x}_{-S}, \boldsymbol{\theta})$. In addition, for any index $i \in S$ it holds:

$$Q_S^i(\boldsymbol{\theta}) = \frac{p(x_i, \mathbf{x}_{-S} | \boldsymbol{\theta})}{p(\mathbf{x}_{-S} | \boldsymbol{\theta})} = \frac{p(\mathbf{x}_{-(S-\{i\})} | \boldsymbol{\theta})}{p(\mathbf{x}_{-S} | \boldsymbol{\theta})} = \frac{D_{S-\{i\}}(\boldsymbol{\theta})}{D_S(\boldsymbol{\theta})}, \quad (10)$$

where for a set S we define $D_S = p(\mathbf{x}_{-S} | \boldsymbol{\theta}) Z(\boldsymbol{\theta})$. We then have:

$$\log Q_S^i(\boldsymbol{\theta}) = \log D_{S-\{i\}}(\boldsymbol{\theta}) - \log D_S(\boldsymbol{\theta}).$$

We now evaluate the gradient of $\log Q_S^i$ at the ground truth natural parameter in the case of an infinite amount of data. To this end, we fix an index j and consider the following lemma:

Lemma 1 *For a set S and an index j , the partial derivative of $\log D_S$ with respect to θ_j evaluated at $\boldsymbol{\theta} \in \mathbb{R}^d$ is:*

$$\frac{\partial \log D_S}{\partial \theta_j}(\boldsymbol{\theta}) = \mathbb{E}_{\boldsymbol{\theta}}(T_j(\mathbf{x}, \mathbf{z}) | \mathbf{x}_{-S})$$

where $\mathbb{E}_{\boldsymbol{\theta}}$ corresponds to the expectation with respect to the exponential family pdf with parameter $\boldsymbol{\theta}$.

Lemma 1 implies that the partial derivative of the logarithm of the restricted partition function is equal to the conditional expectation of the corresponding sufficient statistics. The proof is presented in Section E.3. As a consequence of Lemma 1, the partial derivative of $\log Q_S^i(\boldsymbol{\theta})$ with respect to θ_j can be expressed as:

$$\frac{\partial \log Q_S^i}{\partial \theta_j}(\boldsymbol{\theta}) = \frac{\partial \log D_{S-\{i\}}}{\partial \theta_j}(\boldsymbol{\theta}) - \frac{\partial \log D_S}{\partial \theta_j}(\boldsymbol{\theta}) = \mathbb{E}_{\boldsymbol{\theta}}(T_j(\mathbf{x}, \mathbf{z}) | \mathbf{x}_{-(S-\{i\})}) - \mathbb{E}_{\boldsymbol{\theta}}(T_j(\mathbf{x}, \mathbf{z}) | \mathbf{x}_{-S}).$$

This partial derivative evaluated for the ground truth parameter is then:

$$\frac{\partial \log Q_S^i}{\partial \theta_j}(\boldsymbol{\theta}^*) = \mathbb{E}_{\boldsymbol{\theta}^*} (T_j(\mathbf{x}, \mathbf{z}) | \mathbf{x}_{-(S-\{i\})}) - \mathbb{E}_{\boldsymbol{\theta}^*} (T_j(\mathbf{x}, \mathbf{z}) | \mathbf{x}_{-S}).$$

In the case of an infinite amount of data from the model defined in Equation (8), we switch the expectation of the gradient with the gradient of the expectation to conclude with the law of total expectation:

$$\begin{aligned} \frac{\partial \mathbb{E}_{\boldsymbol{\theta}^*} \log Q_S^i}{\partial \theta_j}(\boldsymbol{\theta}^*) &= \mathbb{E}_{\boldsymbol{\theta}^*} \left\{ \frac{\partial \log Q_S^i}{\partial \theta_j}(\boldsymbol{\theta}^*) \right\} = \mathbb{E}_{\boldsymbol{\theta}^*} \left\{ \mathbb{E}_{\boldsymbol{\theta}^*} (T_j(\mathbf{x}, \mathbf{z}) | \mathbf{x}_{-(S-\{i\})}) - \mathbb{E}_{\boldsymbol{\theta}^*} (T_j(\mathbf{x}, \mathbf{z}) | \mathbf{x}_{-S}) \right\} \\ &= \mathbb{E}_{\boldsymbol{\theta}^*} (T_j(\mathbf{x}, \mathbf{z})) - \mathbb{E}_{\boldsymbol{\theta}^*} (T_j(\mathbf{x}, \mathbf{z})) \\ &= 0. \end{aligned}$$

Consequently, we have:

$$\nabla_{\boldsymbol{\theta}} \mathbb{E}_{\boldsymbol{\theta}^*} \log Q_S^i(\boldsymbol{\theta}^*) = \mathbf{0}.$$

Equation (9) defines the query training objective value as:

$$\bar{J}(\boldsymbol{\theta}) = \frac{1}{2^n - 1} \sum_{\substack{S \subset \{1, \dots, n\} \\ S \neq \emptyset}} \frac{1}{|S|} \sum_{i \in S} \mathbb{E}_{\boldsymbol{\theta}^*} \{ \log Q_S^i(\boldsymbol{\theta}) \}.$$

We then immediately conclude:

$$\nabla_{\boldsymbol{\theta}} \bar{J}(\boldsymbol{\theta}^*) = \mathbf{0}.$$

□

E.2 Proof of Theorem 2

Proof: The following Lemma is an extension of the previous Lemma 1 and is also proved in Section E.3.

Lemma 2 For a set S and two indexes j and ℓ , the second order partial derivative of $\log D_S$ with respect to θ_j and θ_ℓ , evaluated at $\boldsymbol{\theta} \in \mathbb{R}^d$ is:

$$\frac{\partial^2 \log D_S}{\partial \theta_j \partial \theta_\ell}(\boldsymbol{\theta}) = \mathbb{E}_{\boldsymbol{\theta}} (T_j(\mathbf{x}, \mathbf{z}) T_\ell(\mathbf{x}, \mathbf{z}) | \mathbf{x}_{-S}) - \mathbb{E}_{\boldsymbol{\theta}} (T_j(\mathbf{x}, \mathbf{z}) | \mathbf{x}_{-S}) \mathbb{E}_{\boldsymbol{\theta}} (T_\ell(\mathbf{x}, \mathbf{z}) | \mathbf{x}_{-S}).$$

We can consequently express the Hessian of $\log D_S$ as a conditional covariance matrix:

$$\nabla_{\boldsymbol{\theta}}^2 \log D_S(\boldsymbol{\theta}) = \mathbb{E}_{\boldsymbol{\theta}} \{ \mathbf{T}(\mathbf{x}, \mathbf{z}) \mathbf{T}(\mathbf{x}, \mathbf{z})^T | \mathbf{x}_{-S} \} - \mathbb{E}_{\boldsymbol{\theta}} \{ \mathbf{T}(\mathbf{x}, \mathbf{z}) | \mathbf{x}_{-S} \} \mathbb{E}_{\boldsymbol{\theta}} \{ \mathbf{T}(\mathbf{x}, \mathbf{z}) | \mathbf{x}_{-S} \}^T.$$

Similarly, for an index $i \in S$, the Hessian $\nabla_{\boldsymbol{\theta}}^2 \log D_{S-\{i\}}(\boldsymbol{\theta})$ is equal to:

$$\mathbb{E}_{\boldsymbol{\theta}} \{ \mathbf{T}(\mathbf{x}, \mathbf{z}) \mathbf{T}(\mathbf{x}, \mathbf{z})^T | \mathbf{x}_{-(S-\{i\})} \} - \mathbb{E}_{\boldsymbol{\theta}} \{ \mathbf{T}(\mathbf{x}, \mathbf{z}) | \mathbf{x}_{-(S-\{i\})} \} \mathbb{E}_{\boldsymbol{\theta}} \{ \mathbf{T}(\mathbf{x}, \mathbf{z}) | \mathbf{x}_{-(S-\{i\})} \}^T.$$

We evaluate the Hessian of $\log Q_S^i$ at the ground truth parameters $\boldsymbol{\theta}^*$ in the case of an infinite amount of data:

$$\begin{aligned} &\nabla_{\boldsymbol{\theta}}^2 \mathbb{E}_{\boldsymbol{\theta}^*} \{ \log Q_S^i(\boldsymbol{\theta}^*) \} \\ &= \mathbb{E}_{\boldsymbol{\theta}^*} \{ \nabla_{\boldsymbol{\theta}}^2 \log Q_S^i(\boldsymbol{\theta}^*) \} \\ &= \mathbb{E}_{\boldsymbol{\theta}^*} \{ \nabla_{\boldsymbol{\theta}}^2 \log D_{S-\{i\}}(\boldsymbol{\theta}^*) - \nabla_{\boldsymbol{\theta}}^2 \log D_S(\boldsymbol{\theta}^*) \} \\ &= \mathbb{E}_{\boldsymbol{\theta}^*} \left\{ \mathbb{E}_{\boldsymbol{\theta}^*} \{ \mathbf{T}(\mathbf{x}, \mathbf{z}) \mathbf{T}(\mathbf{x}, \mathbf{z})^T | \mathbf{x}_{-(S-\{i\})} \} - \mathbb{E}_{\boldsymbol{\theta}^*} \{ \mathbf{T}(\mathbf{x}, \mathbf{z}) | \mathbf{x}_{-(S-\{i\})} \} \mathbb{E}_{\boldsymbol{\theta}^*} \{ \mathbf{T}(\mathbf{x}, \mathbf{z}) | \mathbf{x}_{-(S-\{i\})} \}^T \right\} \\ &\quad - \mathbb{E}_{\boldsymbol{\theta}^*} \left\{ \mathbb{E}_{\boldsymbol{\theta}^*} \{ \mathbf{T}(\mathbf{x}, \mathbf{z}) \mathbf{T}(\mathbf{x}, \mathbf{z})^T | \mathbf{x}_{-S} \} - \mathbb{E}_{\boldsymbol{\theta}^*} \{ \mathbf{T}(\mathbf{x}, \mathbf{z}) | \mathbf{x}_{-S} \} \mathbb{E}_{\boldsymbol{\theta}^*} \{ \mathbf{T}(\mathbf{x}, \mathbf{z}) | \mathbf{x}_{-S} \}^T \right\} \\ &= \mathbb{E}_{\boldsymbol{\theta}^*} \left\{ \mathbb{E}_{\boldsymbol{\theta}^*} \{ \mathbf{T}(\mathbf{x}, \mathbf{z}) | \mathbf{x}_{-S} \} \mathbb{E}_{\boldsymbol{\theta}^*} \{ \mathbf{T}(\mathbf{x}, \mathbf{z}) | \mathbf{x}_{-S} \}^T \right\} \\ &\quad - \mathbb{E}_{\boldsymbol{\theta}^*} \left\{ \mathbb{E}_{\boldsymbol{\theta}^*} \{ \mathbf{T}(\mathbf{x}, \mathbf{z}) | \mathbf{x}_{-(S-\{i\})} \} \mathbb{E}_{\boldsymbol{\theta}^*} \{ \mathbf{T}(\mathbf{x}, \mathbf{z}) | \mathbf{x}_{-(S-\{i\})} \}^T \right\} \text{ with the law of total expectation.} \end{aligned}$$

For $\mathbf{u} \in \mathbb{R}^d$, we consequently have:

$$\mathbf{u}^T \nabla_{\boldsymbol{\theta}}^2 \mathbb{E}_{\boldsymbol{\theta}^*} \{\log Q_S^i(\boldsymbol{\theta}^*)\} \mathbf{u} = \mathbb{E}_{\boldsymbol{\theta}^*} \left\{ \left(\mathbb{E}_{\boldsymbol{\theta}^*} \{ \mathbf{u}^T \mathbf{T}(\mathbf{x}, \mathbf{z}) | \mathbf{x}_{-S} \} \right)^2 - \left(\mathbb{E}_{\boldsymbol{\theta}^*} \{ \mathbf{u}^T \mathbf{T}(\mathbf{x}, \mathbf{z}) | \mathbf{x}_{-S \cup \{i\}} \} \right)^2 \right\}$$

The first term only depends upon \mathbf{x}_{-S} while the second also depends upon x_i . We can then use properties of the conditional expectation and Jensen's inequality to derive:

$$\begin{aligned} \mathbb{E}_{\boldsymbol{\theta}^*} \left\{ \left(\mathbb{E}_{\boldsymbol{\theta}^*} \{ \mathbf{u}^T \mathbf{T}(\mathbf{x}, \mathbf{z}) | \mathbf{x}_{-S} \} \right)^2 \right\} &= \mathbb{E}_{\boldsymbol{\theta}^*} \left\{ \left(\mathbb{E}_{\boldsymbol{\theta}^*} \left\{ \mathbb{E}_{\boldsymbol{\theta}^*} \{ \mathbf{u}^T \mathbf{T}(\mathbf{x}, \mathbf{z}) | \mathbf{x}_{-S \cup \{i\}} \} | \mathbf{x}_{-S} \right\} \right)^2 \right\} \\ &\leq \mathbb{E}_{\boldsymbol{\theta}^*} \left\{ \mathbb{E}_{\boldsymbol{\theta}^*} \left\{ \left(\mathbb{E}_{\boldsymbol{\theta}^*} \{ \mathbf{u}^T \mathbf{T}(\mathbf{x}, \mathbf{z}) | \mathbf{x}_{-S \cup \{i\}} \} \right)^2 | \mathbf{x}_{-S} \right\} \right\} \\ &= \mathbb{E}_{\boldsymbol{\theta}^*} \left\{ \left(\mathbb{E}_{\boldsymbol{\theta}^*} \{ \mathbf{u}^T \mathbf{T}(\mathbf{x}, \mathbf{z}) | \mathbf{x}_{-S \cup \{i\}} \} \right)^2 \right\}. \end{aligned}$$

We then have:

$$\mathbf{u}^T \nabla_{\boldsymbol{\theta}}^2 \mathbb{E}_{\boldsymbol{\theta}^*} \{\log Q_S^i(\boldsymbol{\theta}^*)\} \mathbf{u} \leq 0, \forall \mathbf{u} \in \mathbb{R}^d.$$

Hence, the symmetric Hessian $\nabla_{\boldsymbol{\theta}}^2 \mathbb{E}_{\boldsymbol{\theta}^*} \{\log Q_S^i(\boldsymbol{\theta}^*)\}$ is negative semidefinite, and so is $\nabla_{\boldsymbol{\theta}}^2 \bar{J}(\boldsymbol{\theta}^*)$. \square

E.3 Proof of Lemmas 1 and 2

Proof: We prove the two Lemmas 1 and 2 simultaneously.

We consider a non-empty subset $S \subset \{1, \dots, n\}$, an index $i \in S$ and an index j . We assume without loss of generality that $S = \{1, \dots, |S|\}$. For an exponential family model with natural parameter $\boldsymbol{\theta} \in \mathbb{R}^d$, we have defined:

$$D_S(\boldsymbol{\theta}) = p(\mathbf{x}_{-S} | \boldsymbol{\theta}) Z(\boldsymbol{\theta}) = \sum_{\substack{\boldsymbol{\xi}_S \in \{1, \dots, K\}^{|S|}, \\ \mathbf{z} \in \{1, \dots, L\}^m}} p(\boldsymbol{\xi}_S, \mathbf{x}_{-S}, \mathbf{z} | \boldsymbol{\theta}) Z(\boldsymbol{\theta}) = \sum_{\boldsymbol{\xi}_S, \mathbf{z}} \prod_{k=1}^d \exp(\theta_k T_k(\boldsymbol{\xi}_S, \mathbf{x}_{-S}, \mathbf{z})),$$

where we have used the model definition in Equation (8). For each term, exactly one factor depends upon θ_j . We consequently evaluate the partial derivative of $\log D_S$ with respect to θ_j :

$$\begin{aligned} \frac{\partial \log D_S}{\partial \theta_j}(\boldsymbol{\theta}) &= \frac{\sum_{\boldsymbol{\xi}_S, \mathbf{z}} T_j(\boldsymbol{\xi}_S, \mathbf{x}_{-S}, \mathbf{z}) \prod_{k=1}^d \exp(\theta_k T_k(\boldsymbol{\xi}_S, \mathbf{x}_{-S}, \mathbf{z}))}{\sum_{\boldsymbol{\xi}_S, \mathbf{z}} \prod_{k=1}^d \exp(\theta_k T_k(\boldsymbol{\xi}_S, \mathbf{x}_{-S}, \mathbf{z}))} \\ &= \sum_{\boldsymbol{\xi}_S, \mathbf{z}} T_j(\boldsymbol{\xi}_S, \mathbf{x}_{-S}, \mathbf{z}) \frac{p(\boldsymbol{\xi}_S, \mathbf{x}_{-S}, \mathbf{z} | \boldsymbol{\theta})}{p(\mathbf{x}_{-S} | \boldsymbol{\theta})}. \end{aligned}$$

We then derive Lemma 1:

$$\frac{\partial \log D_S}{\partial \theta_j}(\boldsymbol{\theta}) = \mathbb{E}_{\boldsymbol{\theta}} (T_j(\mathbf{x}, \mathbf{z}) | \mathbf{x}_{-S}).$$

Let ℓ be another index. A similar computation leads to:

$$\begin{aligned} \frac{\partial^2 \log D_S}{\partial \theta_j \partial \theta_\ell}(\boldsymbol{\theta}) &= \frac{\sum_{\boldsymbol{\xi}_S, \mathbf{z}} T_j(\boldsymbol{\xi}_S, \mathbf{x}_{-S}, \mathbf{z}) T_\ell(\boldsymbol{\xi}_S, \mathbf{x}_{-S}, \mathbf{z}) \prod_{k=1}^d \exp(\theta_k T_k(\boldsymbol{\xi}_S, \mathbf{x}_{-S}, \mathbf{z}))}{\sum_{\boldsymbol{\xi}_S, \mathbf{z}} \prod_{k=1}^d \exp(\theta_k T_k(\boldsymbol{\xi}_S, \mathbf{x}_{-S}, \mathbf{z}))} \\ &\quad - \frac{\sum_{\boldsymbol{\xi}_S, \mathbf{z}} T_j(\boldsymbol{\xi}_S, \mathbf{x}_{-S}, \mathbf{z}) \prod_{k=1}^d \exp(\theta_k T_k(\boldsymbol{\xi}_S, \mathbf{x}_{-S}, \mathbf{z}))}{\sum_{\boldsymbol{\xi}_S, \mathbf{z}} \prod_{k=1}^d \exp(\theta_k T_k(\boldsymbol{\xi}_S, \mathbf{x}_{-S}, \mathbf{z}))} \\ &\quad \times \frac{\sum_{\boldsymbol{\xi}_S, \mathbf{z}} T_\ell(\boldsymbol{\xi}_S, \mathbf{x}_{-S}, \mathbf{z}) \prod_{k=1}^d \exp(\theta_k T_k(\boldsymbol{\xi}_S, \mathbf{x}_{-S}, \mathbf{z}))}{\sum_{\boldsymbol{\xi}_S, \mathbf{z}} \prod_{k=1}^d \exp(\theta_k T_k(\boldsymbol{\xi}_S, \mathbf{x}_{-S}, \mathbf{z}))}. \end{aligned}$$

Hence, we derive Lemma 2:

$$\frac{\partial^2 \log D_S}{\partial \theta_j \partial \theta_\ell}(\boldsymbol{\theta}) = \mathbb{E}_{\boldsymbol{\theta}} (T_j(\mathbf{x}, \mathbf{z}) T_\ell(\mathbf{x}, \mathbf{z}) | \mathbf{x}_{-S}) - \mathbb{E}_{\boldsymbol{\theta}} (T_j(\mathbf{x}, \mathbf{z}) | \mathbf{x}_{-S}) \mathbb{E}_{\boldsymbol{\theta}} (T_\ell(\mathbf{x}, \mathbf{z}) | \mathbf{x}_{-S}).$$

\square